Field-oriented control scheme for linear induction motor with the end effect

G. Kang and K. Nam

Abstract: The movement of a linear induction motor (LIM) causes eddy currents in the secondary conductor sheet at the entry and the exit of the primary core. The eddy currents of the sheet tend to resist sudden flux variation, allowing only gradual change along the airgap. Hence, the so-called 'end effect' causes not only the losses but also airgap flux profile variation changes depending on the speed. In this work, an equivalent circuit model of LIM is developed following Duncan's per phase model. It is then transformed into a synchronous reference frame which is aligned with the secondary flux. Also, a field orientation control scheme is developed which accounts for the end effect. The validity of the proposed LIM model is demonstrated by comparing experimental and simulated voltage current relations. With the proposed control scheme, the (secondary) flux-attenuation problem due to the end effect is shown to be resolved in the high-speed range.

1 Introduction

In a linear induction motor (LIM), the primary winding corresponds to the stator winding of a rotary induction motor (RIM), while the secondary corresponds to the rotor. Normally, the secondary part of a LIM is made of aluminum and steel plates. As the primary moves, a new flux is continuously developed at the entry of the primary yoke, while existing flux disappears at the exit side. Sudden generation and disappearance of the penetrating field causes eddy currents in the secondary plate. This eddy current affects the airgap flux profile in the longitudinal direction. The loss, as well as the flux-profile attenuation, become severer as the speed increases. Such a phenomena is called 'end effect' of LIM.

Many researchers have derived 'per-phase' equivalent circuits reflecting the end effect [1–11]. Field theory was utilised in developing the lumed parameter LIM model [1–4], in which end effect, field diffusion in the secondary sheet, skin effect and back-iron saturation were considered. However, the resulting lumped-parameter models look very complicated for practical use of modelling and control.

Gieras *et al.* [5] and Faiz *et al.* [6] developed an equivalent circuit by superposing the synchronous wave and the pulsating wave caused by the end effect. Nondahl *et al.* [7] derived an equivalent-circuit model from the pole-by-pole method based on winding functions of the primary windings. Several different models were developed from the electromagnetic relation in the airgap through a Fourier-series approach [8–10].

IEE Proceedings online no. 20045185

doi:10.1049/ip-epa:20045185

Paper first received 14th October 2004 and in final revised form 10th March 2005

G. Kang is with the Electric Powertrain System Development Team, Advanced R&D Center, Hyundai Motor Company, 772-1, Changduk-Dong, Whasung City, Kyunggi-Do, 445-850, South Korea

K. Nam is with the Department of Electrical Engineering, Pohang University of Science and Technology, San-31, Hyoja-dong, Pohang, Kyoungbuk, 790-784, South Korea

E-mail: gubae@hyundai-motor.com

Duncan [11] developed the 'per-phase' equivalent circuit by modifying the magnetising branch of the equivalent circuit of the RIM. Noting that the airgap flux grows and decays gradually from the entry and the exit, respectively, he introduced a weighting function with the use of a dimensionless factor Q. Then, the average values were taken to describe the magnetising inductance and the resistance of the eddy loss. In this paper, we transform the Duncan's model into the dq model in a synchronous frame based on the secondary flux and derive a vector control scheme.

2 End effect of linear induction motor

Figure 1*a* shows a view of a LIM. Both generation and decay of the fields cause the eddy current in the secondary sheet. The eddy current in the entry grows very rapidly to mirror the magnetising current, nullifying the airgap flux at the entry. On the other hand, the eddy current at the exit generates a kind of wake field, dragging the moving motion of the primary core. The density profile of the eddy current along the length of LIM looks like Fig. 1*c* [11]. Hence, the resulting magneto motive force (MMF), and thereby airgap flux, looks like Fig. 1*b*. Duncan introduced a dimensionless factor Q, which is defined by

$$Q \triangleq \frac{T_v}{T_y} = \frac{l/v_y}{L_y/R_y} \tag{1}$$

where l, v_y, L_y and R_y are the motor length, velocity, secondary self inductance and secondary resistance, respectively [11]. T_v is the time for the primary core to traverse a point in the rail and $T_y = L_y/R_y$ is the time constant of the secondary circuit. Q represents the motor length for a given speed v_y, but normalised by the secondary time constant. On this basis, the motor length is infinite at zero speed, and will shrink as the speed increases. Note that if we scale the position x' by

$$x \equiv \frac{x'/v_y}{L_y/R_y}$$

the motor airgap resides on the interval, [0, Q]. On this interval, the amplitudes (envelope) of eddy and magnetising

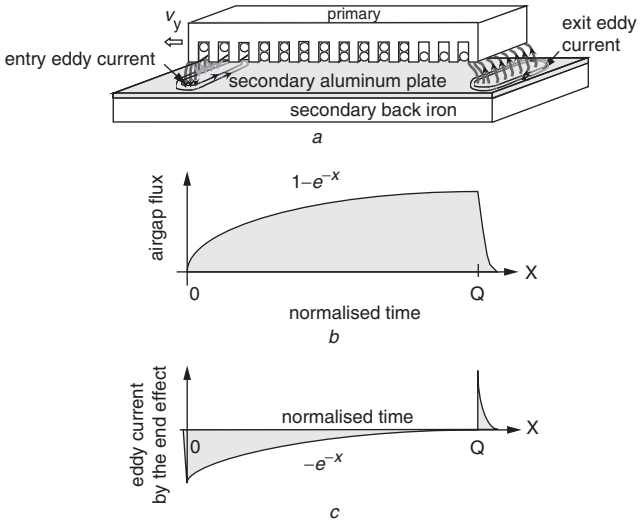

Fig. 1 *Linear induction motor*
a Eddy-current generation at the entry and exit of the airgap when the primary moves with speed v_y
b Airgap flux profile
c Eddy-current density porfile along the length of LIM [11]

currents were assumed to be given by $-I_m e^{-x}$, $I_m(1-\mathrm{e}^{-x})$, respectively. Based on this proposition, Duncan obtained the average values for the eddy current, the magnetising current and secondary eddy loss, and derived a per-phase model [11].

In Duncan's model, the series resistance reflecting the eddy loss appears in the series with the magnetising inductance. The eddy current loss at the entry and exit is, in principle, the same as the core loss. The core loss is normally represented by a parallel resistor to the magnetising inductor [12]. Therefore, the eddy current loss of the secondary conductor also needs to be described by a parallel resistor. However, in Duncan's model, the eddy current loss is described by a series resistor.

As an equivalent-circuit model for LIM with the end effect, consider Fig. 2. Following Duncan's model, let the magnetising inductance be equal to $L_{m0}(1-f(Q))$, where L_{m0} is the magnetising inductance at zero speed and $f(Q)=(1-\mathrm{e}^{-Q})/Q$.

We neglect the eddy-current loss R_{eddy} for the sake of simplicity. However, the inclusion of the loss branch increases the complexity of the equation greatly, whilst the presence or absence of the loss branch does not make a significant difference in the current dynamics unless LIM is moving at a very high speed. Note that only Duncan's magnetising inductance model is utilised here, whilst the resistance R_{eddy} reflecting eddy current loss is neglected.

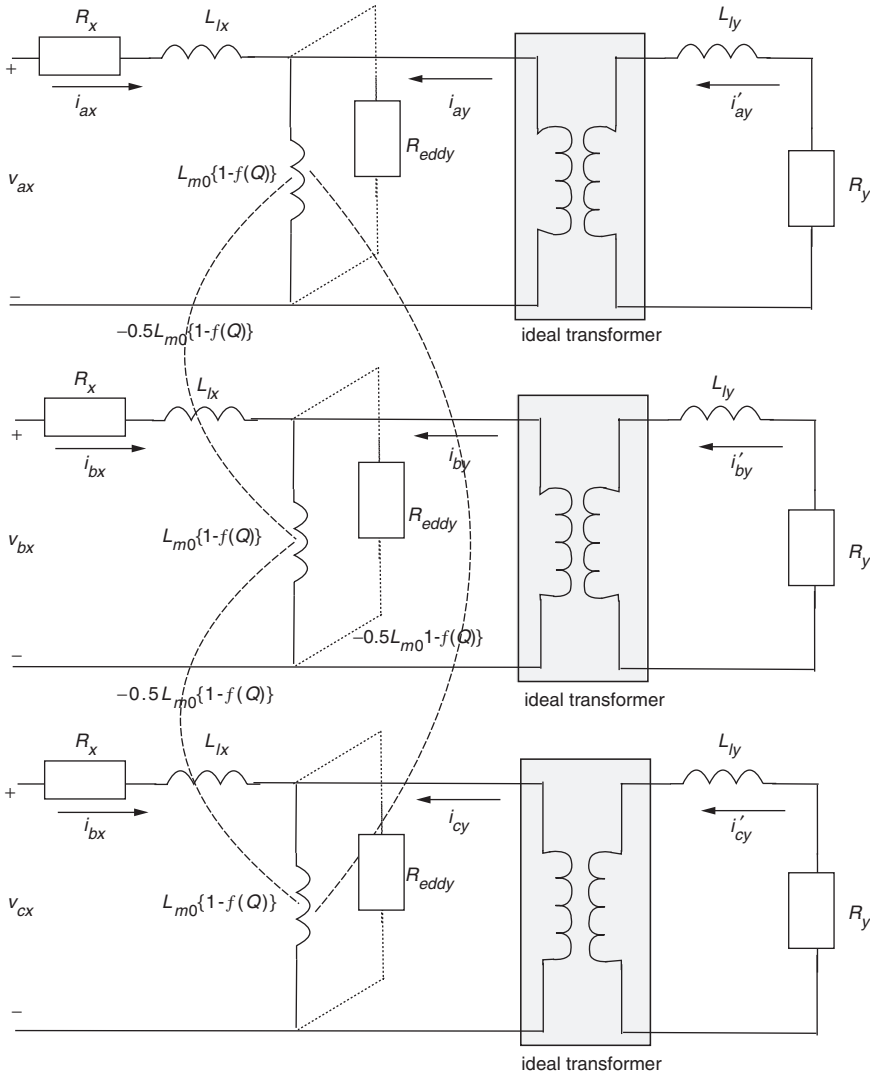

Fig. 2 *Per-phase equivalent circuit of LIM considering the end effect*

The voltage equations of the per-phase model shown in Fig. 2 are given by

$$\boldsymbol{v}_{abcx} = R_x \boldsymbol{i}_{abcx} + p\boldsymbol{\lambda}_{abcx} \tag{2}$$

$$\boldsymbol{v}'_{abcy} = R_y \boldsymbol{i}'_{abcy} + p\boldsymbol{\lambda}'_{abcy} \tag{3}$$

where $\boldsymbol{v}_{abcx} = [v_{ax}\ v_{bx}\ v_{cx}]^T$, $\boldsymbol{i}_{abcx} = [i_{ax}\ i_{bx}\ i_{cx}]^T$ and $\boldsymbol{\lambda}_{abcx} = [\lambda_{ax}\ \lambda_{bx}\ \lambda_{cx}]^T$ are the voltage, current and flux linkage of the primary, and $\boldsymbol{v}'_{abcy} = [v'_{ay}\ v'_{by}\ v'_{cy}]^T$, $\boldsymbol{i}'_{abcy} = [i'_{ay}\ i'_{by}\ i'_{cy}]^T$ and $\boldsymbol{\lambda}'_{abcy} = [\lambda'_{ay}\ \lambda'_{by}\ \lambda'_{cy}]^T$ are the voltage, current and flux of the secondary in the secondary frame. R_x denotes the primary resistance. Further, p denotes the differential operator, d/dt.

To keep the same convention as for the rotary motor, it is assumed that the primary is fixed, while the secondary is moving. The flux-linkage equations for the primary and secondary are given by

$$\boldsymbol{\lambda}_{abcx} = (\boldsymbol{L}_{lx} + \boldsymbol{L}_{mx})\boldsymbol{i}_{abcx} + \boldsymbol{L}_{my}\boldsymbol{i}'_{abcy} \tag{4}$$

$$\boldsymbol{\lambda}'_{abcy} = (\boldsymbol{L}_{ly} + \boldsymbol{L}_{mx})\boldsymbol{i}'_{abcy} + \boldsymbol{L}_{my}{}^T\boldsymbol{i}'_{abcx} \tag{5}$$

where

$$\boldsymbol{L}_{lx(ly)} = \begin{bmatrix} L_{lx(ly)} & 0 & 0 \\ 0 & L_{lx(ly)} & 0 \\ 0 & 0 & L_{lx(ly)} \end{bmatrix}$$

$$\boldsymbol{L}_{mx} = \boldsymbol{L}_{m0}(1 - f(Q)) \begin{bmatrix} 1 & -\frac{1}{2} & -\frac{1}{2} \\ -\frac{1}{2} & 1 & -\frac{1}{2} \\ -\frac{1}{2} & -\frac{1}{2} & 1 \end{bmatrix}$$

$$\boldsymbol{L}_{my} = \boldsymbol{L}_{m0}(1 - f(Q)) \begin{bmatrix} \cos\theta_y & \cos\left(\theta_y + \frac{2\pi}{3}\right) & \cos\left(\theta_y - \frac{2\pi}{3}\right) \\ \cos\left(\theta_y - \frac{2\pi}{3}\right) & \cos\theta_y & \cos\left(\theta_y + \frac{2\pi}{3}\right) \\ \cos\left(\theta_y + \frac{2\pi}{3}\right) & \cos\left(\theta_y - \frac{2\pi}{3}\right) & \cos\theta_y \end{bmatrix}$$

$L_{lx(ly)}$ denotes the primary (secondary) leakage inductance and θ_y is the angular displacement of the secondary.

Co-ordinates are changed into a synchronous reference frame with the following transformation map:

$$\begin{bmatrix} f^e_{dx} \\ f^e_{qx} \end{bmatrix} = \frac{2}{3} \begin{bmatrix} \cos\omega_e t & \sin\omega_e t \\ -\sin\omega_e t & \cos\omega_e t \end{bmatrix} \times \begin{bmatrix} 1 & -\frac{1}{2} & -\frac{1}{2} \\ 0 & \frac{\sqrt{3}}{2} & -\frac{\sqrt{3}}{2} \end{bmatrix} \begin{bmatrix} f_{ax} \\ f_{bx} \\ f_{cx} \end{bmatrix} \tag{6}$$

where ω_e is the electrical angular velocity and f is v, i or λ. Utilising the transformation map (6), we obtain from (2) and (3) such that

$$v^e_{dx} = R_x i^e_{dx} + p\lambda^e_{dx} - \omega_e \lambda^e_{qx} \tag{7}$$

$$v^e_{qx} = R_x i^e_{qx} + p\lambda^e_{qx} + \omega_e \lambda^e_{dx} \tag{8}$$

$$v^e_{dy} = R_y i^e_{dy} + p\lambda^e_{dy} (\omega_e - \omega_y)\lambda^e_{qy} \tag{9}$$

$$v^e_{qy} = R_y i^e_{qy} + p\lambda^e_{qy} + (\omega_e - \omega_y)\lambda^e_{dy} \tag{10}$$

where $(v^e_{dx},\ v^e_{qx})$, $(i^e_{dx},\ i^e_{qx})$ and $(\lambda^e_{dx},\ \lambda^e_{qx})$ are the dq-axis voltages, currents and flux linkages of the primary, and $(v^e_{dy},\ v^e_{qy})$, $(i^e_{dy},\ i^e_{qy})$ and $(\lambda^e_{dy},\ \lambda^e_{qy})$ are the dq-axis voltages, currents and fluxes of the secondary in the secondary frame. ω_y denotes the secondary angular speed. The superscript e on v, i, or λ denotes the quantity in the synchronous reference frame. The dq-axis flux linkages of the primary and secondary are given by

$$\lambda^e_{dx} = L_{lx} i^e_{dx} + L_m\{1 - f(Q)\}(i^e_{dx} + i^e_{dy}) \tag{11}$$

$$\lambda^e_{qx} = L_{lx} i^e_{qx} + L_m\{1 - f(Q)\}(i^e_{qx} + i^e_{qy}) \tag{12}$$

$$\lambda^e_{dy} = L_{ly} i^e_{dy} + L_m\{1 - f(Q)\}(i^e_{dx} + i^e_{dy}) \tag{13}$$

$$\lambda^e_{qy} = L_{ly} i^e_{qy} + L_m\{1 - f(Q)\}(i^e_{qx} + i^e_{qy}) \tag{14}$$

where $L_m = 1.5L_{m0}$.

We further assume that the reference frame is aligned to the secondary flux, i.e. we use the secondary flux-orientation scheme. Then, $\lambda^e_{qy} = \dot{\lambda}^e_{qy} = 0$. With $v^e_{dy} = v^e_{qy} = 0$, we obtain from (7)–(10) such that

$$pi^e_{dx} = -\frac{R_x}{L_\sigma(Q)} i^e_{dx} + \frac{1}{L_\sigma(Q)} v^e_{dx} + \omega_e i^e_{qx} \tag{15}$$

$$pi^e_{qx} = -\frac{R_x}{L_\sigma(Q)} i^e_{qx} + \frac{1}{L_\sigma(Q)} v^e_{qx} - \omega_e \left[i^e_{dx} + \frac{L_m(1 - f(Q))}{L_\sigma(Q)\{L_y - L_m f(Q)\}} \lambda^e_{dy} \right] \tag{16}$$

$$\lambda^e_{dy} = \frac{L_m\{1 - f(Q)\}}{1 + \{T_y - L_m f(Q)/R_y\}p} i^e_{dx} \tag{17}$$

$$\omega_{sl} = \frac{L_m\{1 - f(Q)\} i^e_{qx}}{\{T_y - L_m f(Q)/R_y\}\lambda^e_{dy}} \tag{18}$$

where the total leakage inductance is denoted by

$$L_\sigma(Q) = L_x - L_m f(Q) - \frac{[L_m\{1 - f(Q)\}]^2}{L_y - L_m f(Q)}$$

and $\omega_{sl} \equiv \omega_e - \omega_y$, the slip angular frequency. Note that if $v_y \simeq 0$ with $f(Q) \simeq 0$, then $\omega_{sl} \simeq L_m i^e_{qx}/(T_y \lambda^e_{dy})$ and $\lambda^e_{dy} \simeq L_m i^e_{dx}/(1 + T_y p)$ which are the cases of RIM. Note from (17) that λ^e_{dy} for a given i^e_{dx} decreases as LIM velocity v_y increases since $f(Q) \to 1$ as $v_y \to \infty$. This decrease of the magnetising inductance is an illustration of the airgap flux attenuation due to the end effect. Hence, to keep the flux constant, i^e_{dx} needs to be compensated as motor speed increases.

On the other hand, input power P_{in} is obtained from (7)–(10) such that

$$\begin{aligned} P_{in} &= \frac{3}{2}\left(v^e_{dx} i^e_{dx} + v^e_{qx} i^e_{qx} + v^e_{dy} i^e_{dy} + v^e_{qy} i^e_{qy}\right) \\ &= \frac{3}{2}\left(R_x\left(i^{e\,2}_{dx} + i^{e\,2}_{qx}\right) + R_y\left(i^{e\,2}_{dy} + i^{e\,2}_{qy}\right)\right. \\ &\quad + p\left[\frac{L_{lx}}{2}\left(i^{e\,2}_{dx} + i^{e\,2}_{qx}\right) + \frac{L_{ly}}{2}\left(i^{e\,2}_{dy} + i^{e\,2}_{qy}\right)\right. \\ &\quad \left. + L_m\{1 - f(Q)\}\left\{\left(i^e_{dx} + i^e_{dy}\right)^2 + \left(i^e_{qx} + i^e_{qy}\right)^2\right\}\right] \\ &\quad \left. + \left[\omega_r L_m\{1 - f(Q)\}\left(i^e_{qx} i^e_{dy} - i^e_{dx} i^e_{qy}\right)\right]\right) \end{aligned} \tag{19}$$

Note that the electrical power into the terminals of LIM can be divided into three groups. The first group accounts

for the power dissipated in the primary and secondary resistances. The second group corresponds to the time rate of the magnetic energy stored in the inductances. The last group $P_{em} \equiv 1.5\omega_r L_m\{1-f(Q)\}(i^e_{qx}i^e_{dy} - i^e_{dx}i^e_{qy})$ is the electromechanical output power being converted from electrical to mechanical form. Since P_{em} is equal to the product of speed and torque, thrust F is obtained from (13) and (14) such that

$$F = \frac{\pi}{\tau}\frac{P_{em}}{\omega_m} = \frac{3}{2}\frac{P}{2}\frac{\pi}{\tau}\frac{L_m\{1-f(Q)\}}{L_y - L_m f(Q)}\lambda^e_{dy} i^e_{qx} \tag{20}$$

where τ denotes the pole pitch and ω_m the mechanical angular speed, i.e. $\omega_m = (2/P)\omega_r$. In deriving the above thrust equation, it was assumed that $\lambda^e_{qy} = 0$ with the secondary flux-orientation scheme.

Since $L_y = L_m + L_{ly}, L_y \simeq L_m$ if the leakage inductance $L_{ly} \ll L_m$. In this case $1-f(Q)$ cancels out, and thereby F does not directly depend on Q. Therefore, the dependence of F on the speed appears not to be so significant as far as λ^e_{dy} is kept constant. It will be shown in the later simulation part that dependence of λ^e_{dy} on Q is large, while dependence of F on Q is small.

3 Field-orientation control based on secondary flux

In Section 2, we developed a *dq* dynamic model for LIM with the end effect. In this Section, we construct a speed and thrust controller based on the proposed model.

3.1 Flux and thrust controllers

With the classical vector control, secondary flux is linearly proportional to primary *d*-axis current in the steady state, i.e. $\lambda^e_{dy} = L_m i^e_{dx}$. However, with the proposed model the coefficient depends strongly on the velocity, i.e. it follows from (17) that $\lambda^e_{dy} = L_m(1-f(Q))i^e_{dx}$ in the steady state. Although the coefficient varies with velocity, it still holds linear proportionality, and a proportional–integral (PI) controller performs well for this case unless the rate of change of Q is fast. However, the point is how to estimate the flux for the feedback. Utilising (17), we obtain a flux controller such that

$$\begin{aligned} i^{e*}_{dx} &= (PI_1)\left(\lambda^{e*}_{dy} - \hat{\lambda}^e_{dy}\right) \\ &= (PI_1)\left[\lambda^{e*}_{dy} - \frac{L_m\{1-f(Q)\}}{1+\{T_y - L_m f(Q)/R_y\}p} i^e_{dx}\right] \end{aligned} \tag{21}$$

where PI_1 denotes a PI controller of the type $(K_P + K_I/p)$ for some K_P, $K_I > 0$, i^{e*}_{dx} is a *d*-axis primary current command, λ^{e*}_{dy} is a *d*-axis secondary flux command, and $\hat{\lambda}^e_{dy}$ is an estimate of λ^e_{dy}. The flux estimate is equivalently expressed as

$$p\hat{\lambda}^e_{dy} = -\frac{R_y}{L_y - L_m f(Q)}\hat{\lambda}^e_{dy} + \frac{R_y L_m\{1-f(Q)\}}{L_y - L_m f(Q)} i^e_{dx}. \tag{22}$$

Similarly to the ordinary vector-control case, a thrust controller is developed with a PI controller such that

$$\begin{aligned} i^{e*}_{qx} &= (PI_2)(F^* - \hat{F}) \\ &= (PI_2)\left[F^* - \frac{3}{2}\frac{P}{2}\frac{\pi}{\tau}\frac{L_m\{1-f(Q)\}}{L_y - L_m f(Q)}\hat{\lambda}^e_{dy} i^e_{qx}\right] \end{aligned} \tag{23}$$

where PI_2 denotes another PI controller, i^{e*}_{qx} is a *q*-axis primary current command, F^* is a thrust command, and $\hat{F}$ is an estimate of the thrust.

3.2 Current controller

The primary currents are regulated by a PI controller (PI_3) with decoupling and back-EMF compensation terms such that

$$v^e_{dx} = (PI_3)\left(i^{e*}_{dx} - i^e_{dx}\right) - \omega_e L_\sigma(Q) i^e_{qx} \tag{24}$$

$$\begin{aligned} v^e_{qx} &= (PI_3)\left(i^{e*}_{qx} - i^e_{qx}\right) + \omega_e L_\sigma(Q) i^e_{dx} \\ &\quad + \omega_e \frac{L_m\{1-f(Q)\}}{L_y - L_m f(Q)}\hat{\lambda}^e_{dy}. \end{aligned} \tag{25}$$

The overall proposed control block diagram and LIM model appear in Fig. 3. Recall that the end effect is counted in both the LIM model and the controller through Q.

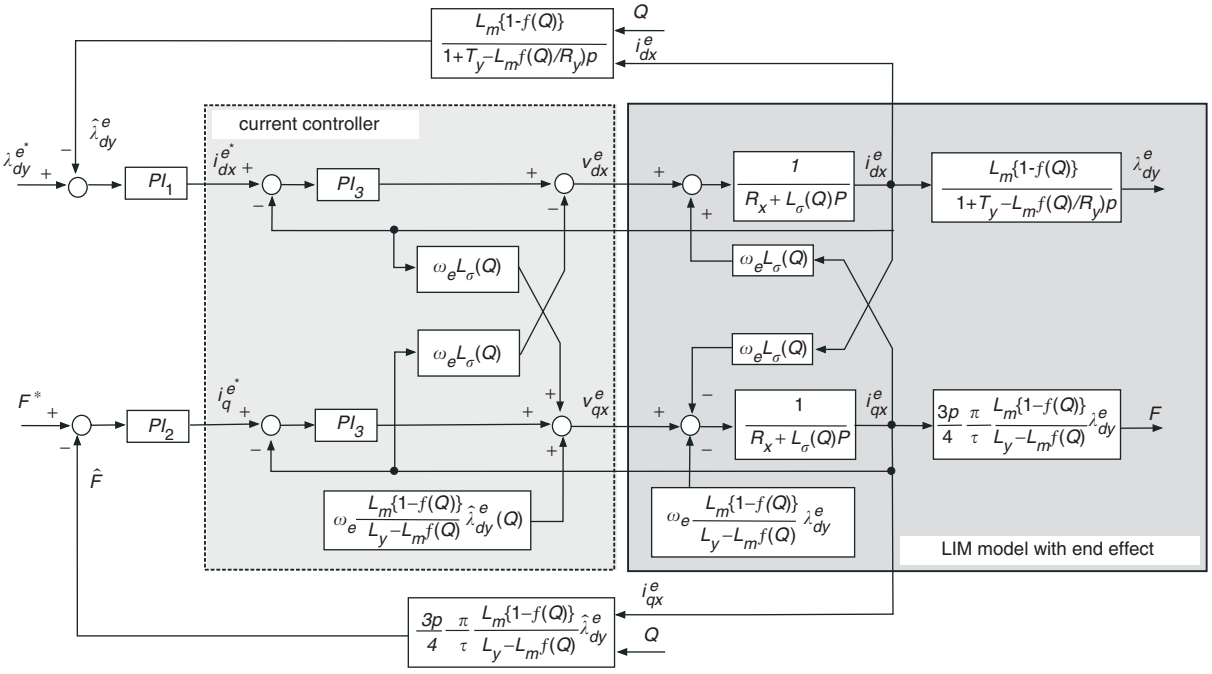

Fig. 3 *Proposed controller and LIM model considering the end effect*

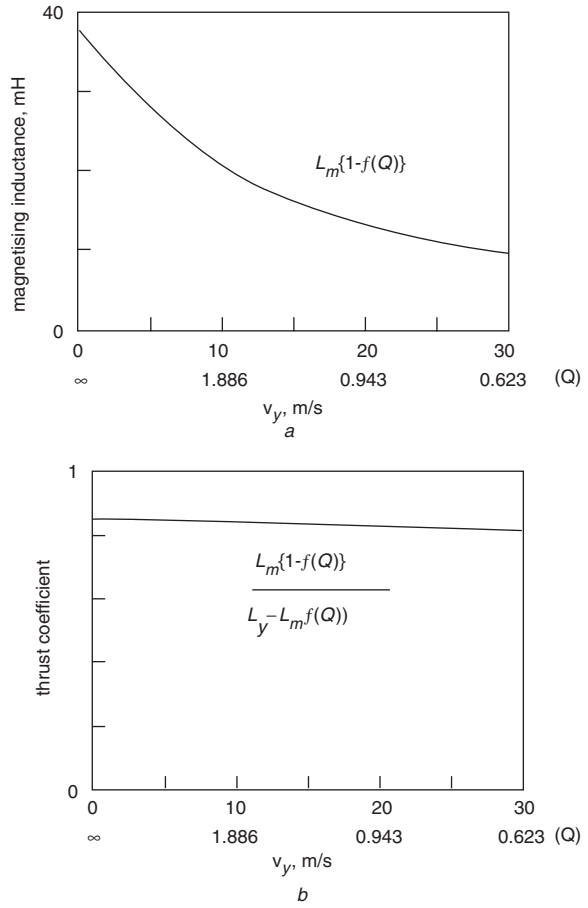

Fig. 4 *Magnetising inductance and thrust coefficient*
a Magnetising inductance against speed
b Thrust coefficient against speed

4 Simulation and experimental results

4.1 Simulation results

For the simulation study, we use (2)–(5) in the *a–b–c* frame as a LIM model. Simulation was performed with the measured parameters of a real LIM that were utilised in the experiment. The measured parameters were: $L_{lx} = 22.5\,\text{mH}$, $L_{ly} = 6.5\,\text{mH}$, $L_m = 37.6\,\text{mH}$, $R_x = 1.2\,\Omega$, $R_y = 2.7\,\Omega$ and motor power = 4.4 kVA.

Figure 4 shows the magnetising inductance $L_m\{1-f(Q)\}$ and thrust coefficient $L_m\{1-f(Q)\}/\{L_y - L_m f(Q)\}$ against speed. A noticeable reduction of the magnetising inductance is observed with increase of v_y, whereas the thrust coefficient remains almost invariant. This supports the observation mentioned in the last part of Section 2. Specifically, the magnetising inductance reduces to about a half of the starting value at a speed of 10 m/s.

Figure 5 presents simulation results showing the responses to a rectangular shape-thrust command. Figure 5*a* shows the plots of thrust, primary currents, secondary flux and speed when the conventional vector control is applied, whereas Fig. 5*b* shows the same things when the proposed control is applied. The term 'conventional vector control' implies the field-oriented control without a provision for the end effect. With the conventional vector control, flux level decreases as the speed increases. Correspondingly, the thrust also decreases, yielding lower speed. On the other hand, with the proposed scheme the flux level is kept constant and no discrepancy is observed between the thrust command and the produced thrust. Note however, that the *d*-axis-current command level increases with the speed to compensate for the end effect. The proposed scheme produces a higher final speed.

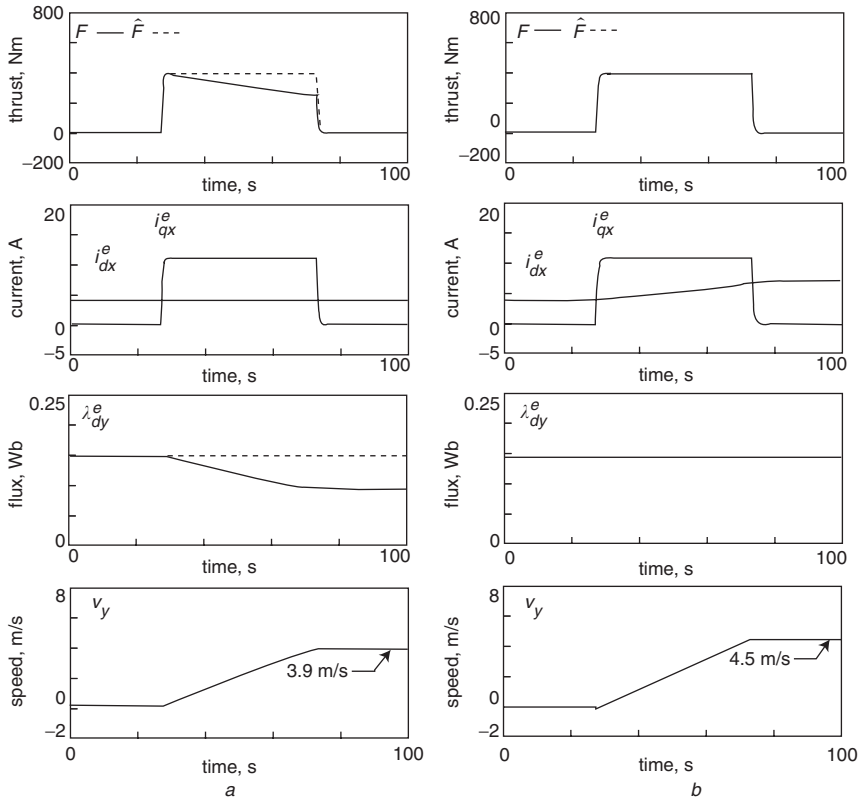

Fig. 5 *Simulation results when a square shape-thrust command is applied*
F = thrust, i^e_{dx}, i^e_{dy} = primary currents, λ^e_{dy} = secondary current, v_y = speed
a Conventional control
b Proposed control

4.2 Experimental results

The linear motor used in this experiment is shown in Fig. 6. The primary yoke was mounted on a fixed pole, while the secondary circuit comprising aluminum plate and steel was mounted on a big flywheel. The dimensions of the LIM are shown in Table 1. Figure 7 shows a block diagram illustrating the proposed vector control. In Fig. 7, PI gains for the flux, thrust and current controllers were selected as $PI_1 = (200p + 100000)/p$, $PI_2 = (0.015p + 15)/p$, and $PI_3 = (25p = 80000)/p$, respectively.

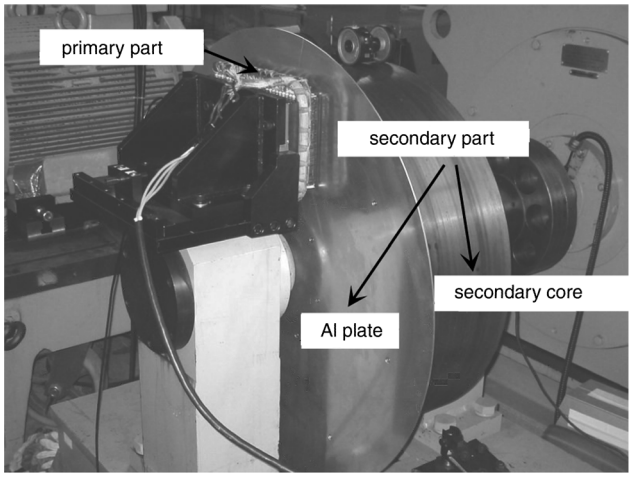

Fig. 6 *LIM with a disk-type secondary plate used in this experiment*

Table 1: Dimensions of a single-side LIM

Motor length, width	0.308 m, 0.170 m	Series turns/phase	240
Pole pitch	0.066 m	Primary back iron	15 mm
Number of poles	4	Effective airgap	6.6 mm
Slots per pole	6	Secondary sheet	3 mm aluminum
Coil pitch	5	Q	$18.86/v_y$

The validity of the proposed model is demonstrated first by comparing the measured current and the calculated currents based on two models, while increasing the speed. Figure 8 shows the currents in the steady state at each speed for the same voltage inputs: Fig. 8 shows real measured currents i^e_{dx} , i^e_{qx}, the calculated currents $\hat{i}^e_{dx}$, $\hat{i}^e_{qx}$ based on the proposed model (15)–(18), and the calculated $\bar{i}^e_{dx}, \bar{i}^e_{qx}$ based on the conventional model without the end effect. Note that the proposed model produced results very close to the experimental results, while the conventional model showed big difference as the speed increased.

Figure 9 shows the experimental results when the same rectangular shape-thrust command was applied. The experimental results look quite close to the simulation results shown in Fig. 5. Note again that the conventional control results in a decrease in flux as the speed increases, but the proposed control yields constant flux by injecting more i^e_{dx}.

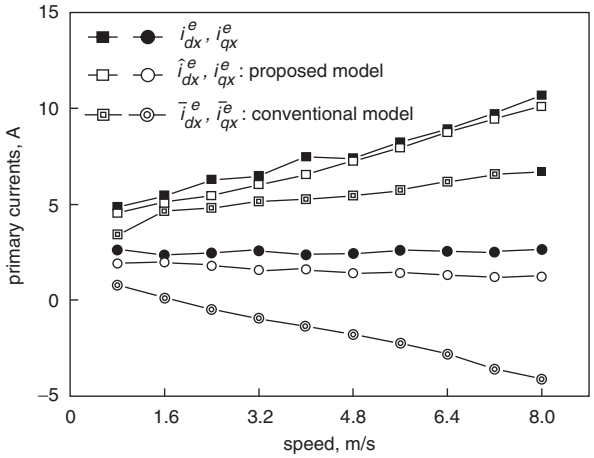

Fig. 8 *Experimental results*
Measured currents i^e_{dx}, i^e_{qx}, calculated currents $\hat{i}^e_{dx}, \hat{i}^e_{qx}$ based on the proposed model, and calculated currents $\bar{i}^e_{dx}, \bar{i}^e_{qx}$ based on the conventional model without the end effect. All steady-state values for the same voltage inputs at each speed.

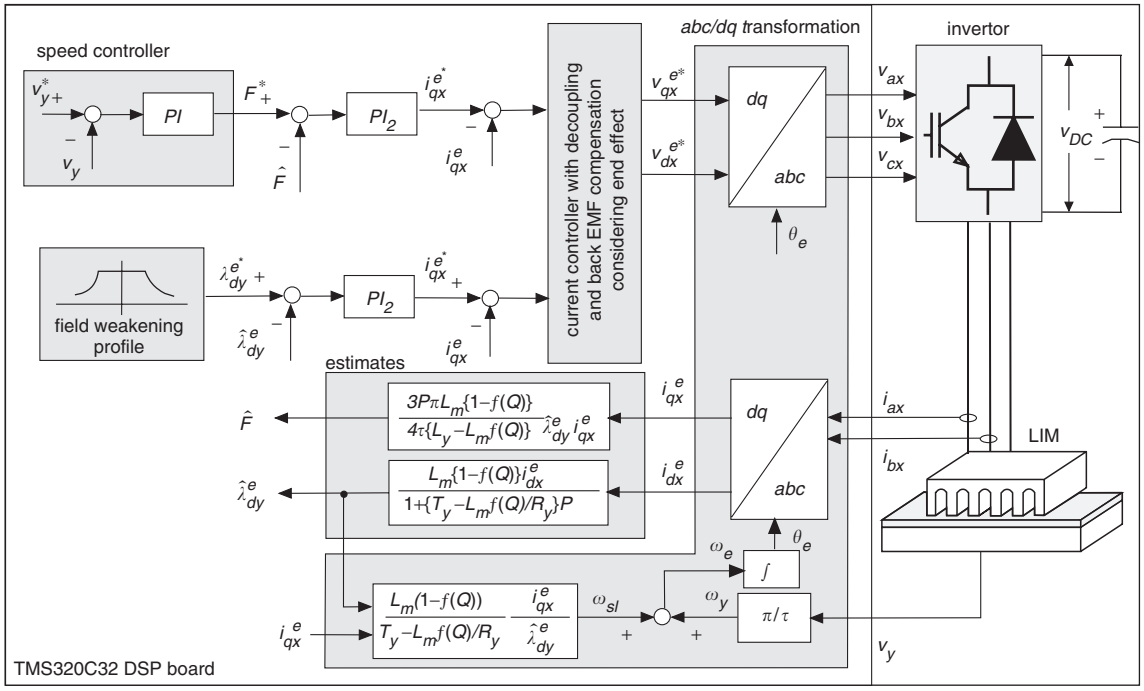

Fig. 7 *Block diagram of the proposed vector-control scheme considering the end effect*

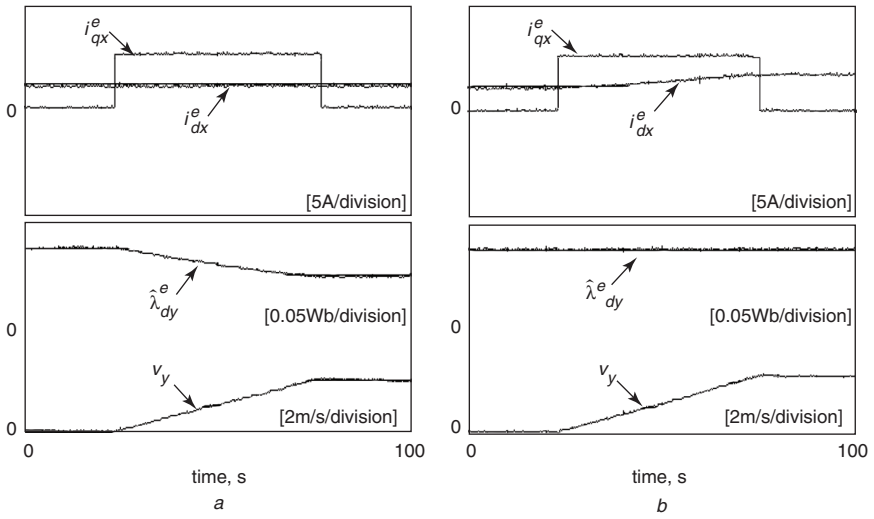

Fig. 9 *Experimental results*
Primary currents i^e_{dx}, i^e_{qx}, secondary flux λ^e_{dy}, and motor speed v_y when a rectangular shape thrust command is applied
a Conventional control
b Proposed control

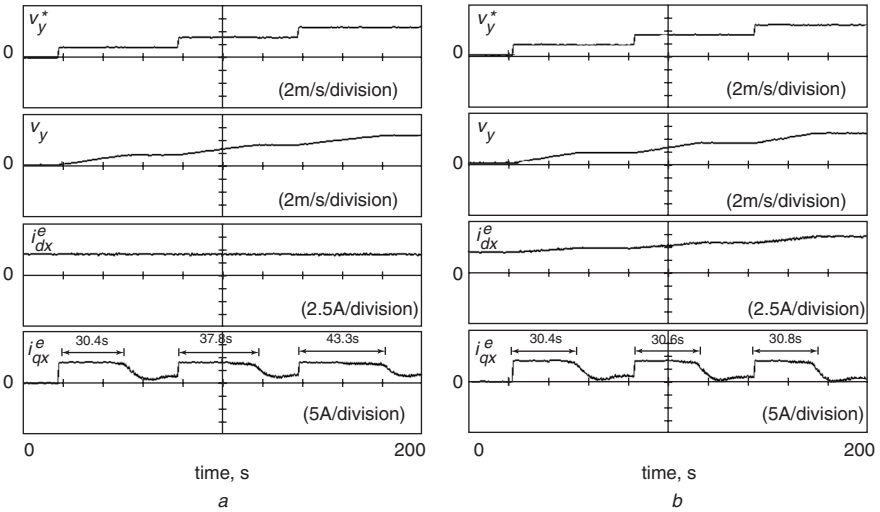

Fig. 10 *Experimental results*
Motor-speed command v^*_y, motor speed v_y, and primary currents i^e_{dx}, i^e_{qx} when a staircase speed command, [0, 1.6, 3.2, 4.8] m/s is applied
a Conventional control
b Proposed control

Figure 10 shows the experimental results when a staircase speed command, [0, 1.6, 3.2, 4.8] m/s was applied. At this time LIM was running in a speed-control mode. Shown in the last row are the acceleration periods and the duration of injecting the maximum i^e_{qx}. With the conventional controller, the period gets longer and longer as the speed increases. The reason is that the flux level, and consequently the thrust, decreases as the speed increases. In Fig. 10*b* the acceleration period is almost identical irrespective of speed with the proposed control method. This indirectly proves the effectiveness of the proposed control scheme that decouples flux level from speed, i.e. the flux level is made independent of the speed.

5 Concluding remarks

The end effect of LIM causes profile change and attenuation of the airgap flux. This becomes more severe as the speed increases. In this work Duncan's model is modified into the *d-q* frame and the field-oriented control scheme aligned with the secondary flux was developed. Both flux and thrust coefficient were expressed with Q. However, it was observed in the LIM model that the dependence of the flux on Q was great, whereas the dependence of the thrust coefficient on Q was not so significant. The validity of the LIM model was checked by comparing currents from an experiment with those from the models. A vector controller was developed based on the proposed model. Experiments were performed in the thrust-control mode, as well as in the speed control mode. In both cases, the problem of flux attenuation caused by speed (eddy current) increase was not observed with the proposed control scheme.

6 References

1 Dawson, G.E., Eastham, A.R., and Gieras, J.F.: 'Design of linear induction drives by fields analysis and finite-element techniques', *IEEE. Trans.*, 1986, **IA-22**, (5), pp. 865–873

2 Pai, R.M., Boldea, I., and Nasar, S.A.: 'A complete equivalent circuit of a linear induction motor with sheet secondary', *IEEE. Trans.*, 1988, **MAG-24**, (1), pp. 639–654
3 Gerias, J.F., Eastham, A.R., and Dawson, G.E.: 'Performance calculation for single-sided linear induction motors with solid steel reaction plate under constant current excitation', *IEEE. Proc. Electr. Power Appl.*, 1985, **132**, (4), pp. 185–194
4 Idir, K., Dawson, G.E., and Eastham, A.R.: 'Modeling and performance of linear induction motor with saturable primary', *IEEE. Trans.*, 1993, **IA-29**, (6), pp. 1123–1128
5 Gieras, J.F., Dawson, G.E., and Eastham, A.R.: 'A new longitudinal end effect factor for linear induction motors', *IEEE. Trans.*, 1987, **EC-22**, (1), pp. 152–159
6 Faiz, J., and Jafari, H.: 'Accurate Modeling of single-sided linear induction motor considers end effect and equivalent thickness', *IEEE. Trans.*, 2000, **MAG-36**, (5), pp. 3785–3790
7 Nondahl, T.A., and Novotny, D.W.: 'Three-phase pole-by-pole model of a linear induction machine', *IEE Proc. Elect. Power Appl.*, 1980, **127**, (2), pp. 68–82
8 Yoshida, K. *et al.*: 'New transfer-matrix theory of linear induction machines, taking into account longitudinal and transverse ferromagnetic end effects', *IEE Proc. Elect. Power Appl.*, 1983, **128**, (5), pp. 225–236
9 Balchin, M.J., and Eastham, J.F.: 'Model for transients in linear induction machines', *IEEE. Trans.*, 1997, **MAG-33**, (5), pp. 4191–4193
10 Mori, Y., Torii, S., and Ebihara, D.: 'End effect analysis of linear induction motor based on the wavelet transform technique', *IEEE. Trans.*, 1997, **MAG-33**, (5), pp. 4191–4193
11 Duncan, J., and Eng, C.: 'Linear induction motor-equivalent circuit model', *IEE Proc., Electr. Power Appl.*, 1983, **130**, (1), pp. 51–57
12 Levi, E., Boglietti, A., and Pastrorelli, M.: 'Iron loss in rotor-flux-oriented induction machine: Identification, assessment of detuning, and compensation', *IEEE. Trans.*, 2002, **PE-38**, (2), pp. 1365–1370